A Trapezoidal Current Mode to Reduce Peak Current in Near-CRM for Three-Level DC–DC Converter

Zhigang Yao, *Member, IEEE*, Xinyu He, Haogang Lan, Haoxin Yang, *Member, IEEE*, Ziheng Xiao, *Member, IEEE*, Fei Deng, *Member, IEEE*, Caisheng Wang, *Senior Member, IEEE*, and Yi Tang, *Senior Member, IEEE*

***Abstract*—Triangular current mode (TCM) and near-critical conduction mode (near-CRM) are popularly used in dc–dc converters to achieve zero-voltage switching (ZVS). However, they encounter a huge peak current problem, more than twice the average current. To solve this problem, this article proposes a novel trapezoidal current mode (TZCM) for three-level dc–dc converters, aiming to reduce the inductor peak current and realize ZVS simultaneously. A trapezoidal modulation with 2-1-0 level sequences and duty cycle swapping is developed to generate the trapezoidal inductor current. To take advantage of the TZCM, a variable switching frequency control is proposed to realize ZVS for all switches in the full operating range. Compared with TCM, the proposed TZCM and its modulation not only reduce the conduction and turn-OFF losses of the power switches by lowering the peak and rms currents but also realize ZVS at $D = 0.5$, where ZVS cannot be realized in the traditional modulation because the inductor current ripple is equal to zero. The proposed TZCM and variable switching frequency control are validated using a 2-kW prototype with 99.06% efficiency.**

***Index Terms*—Critical conduction mode (CRM), three-level DC–DC converter, trapezoidal modulation, triangular current mode (TCM), zero-voltage switching (ZVS).**

I. Introduction

THE use of high-efficiency dc–dc converters is essential in various applications, such as PV generation, fuel cells, electric vehicle battery charging, and dc loads. To reduce the voltage stress of power switches, multilevel dc–dc topologies have garnered considerable attention due to their superior performance, which not only improves the voltage level of the converter but also reduces the size of the inductor and capacitor in the converter [1]. Among these topologies, the three-level dc–dc converters are particularly favored due to their simple structure [2], [3].

Three-level dc–dc converters have the advantage of reducing the voltage stress of power switches to half of the dc bus voltage and are widely used to increase the rated voltage of the converter [4]. Traditionally, the three-level dc–dc converters are operated in continuous conduction mode (CCM), but this causes hard-switching operation, resulting in significant switching losses and electromagnetic interference problems [5], [6]. To overcome these drawbacks, literature [7], [8], [9] have studied soft-switching techniques, especially zero-voltage switching (ZVS), which is a favorable method to eliminate the turn-ON and diode reverse recovery losses and is widely used in power electronic converters. For the traditional methods, some auxiliary components and circuits need to be added to the original power converter to realize the ZVS, resulting in increased hardware complexity and size [10]. For example, in [11], [12], and [13], some inductors, capacitors, and power semiconductor switches are added to create a resonant transition to realize ZVS.

To avoid the increased auxiliary circuits, the triangular current mode (TCM) is used to achieve ZVS by enlarging the inductor current ripple [14], [15], [16]. For example, in the literature [17], the flying capacitor dc–dc converter is controlled in TCM to realize ZVS without any auxiliary components. However, this mode has a large negative current and peak-to-peak current, resulting in large conduction losses and turn-OFF losses. Therefore, the near-critical conduction mode (near-CRM) is used in [6] and [18] to reduce the inductor peak and rms currents while enabling ZVS by utilizing smaller valley current values. In the literature [5], [6], [19], a three-level dc–dc converter is controlled in near-CRM to realize ZVS without any auxiliary devices. The near-CRM is also applied in a three-level inverter in [20], where the soft-switching is achieved by the fully digital control approach based on variable turn-OFF time and deadtime.

Although ZVS can be realized by controlling the converter in TCM or near-CRM, the peak value of the triangular inductor current is more than twice the average current, which aggravates the current stress and turn-OFF losses of the power switch. To

Manuscript received 9 January 2024; revised 21 April 2024; accepted 4 May 2024. Date of publication 10 May 2024; date of current version 20 June 2024. This work was supported in part by the National Natural Science Foundation of China under Grant 52107210, in part by the Science & Technology Innovation Program of Sichuan Province under Grant 2022NSFSC1899, and in part by Chengdu Guojia Electrical Engineering Company Ltd. under Grant NEEC-2022-B15. Recommended for publication by Associate Editor M. Andersen. *(Corresponding author: Yi Tang.)*

Zhigang Yao is with the School of Electrical Engineering, Southwest Jiaotong University, Chengdu 611756, China, and also with the Energy Research Institute, Nanyang Technological University, Singapore 639798 (e-mail: zhigangyao@swjtu.edu.cn).

Xinyu He and Haogang Lan are with the School of Electrical Engineering, Southwest Jiaotong University, Chengdu 611756, China (e-mail: hxy515@my.swjtu.edu.cn; lanhaogang@my.swjtu.edu.cn).

Haoxin Yang, Ziheng Xiao, and Fei Deng are with the Energy Research Institute, Nanyang Technological University, Singapore 639798 (e-mail: haoxin.yang@ntu.edu.sg; ziheng.xiao@ntu.edu.sg; fei.deng@ntu.edu.sg).

Caisheng Wang is with the Department of Electrical and Computer Engineering, Wayne State University, Detroit, MI 48202 USA (e-mail: cwang@wayne.edu).

Yi Tang is with the School of Electrical and Electronic Engineering, Nanyang Technological University, Singapore 639798 (e-mail: yitang@ntu.edu.sg).

Color versions of one or more figures in this article are available at https://doi.org/10.1109/TPEL.2024.3399216.

Digital Object Identifier 10.1109/TPEL.2024.3399216

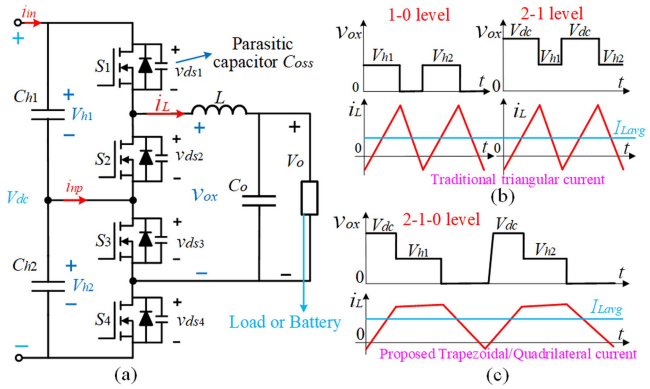

Fig. 1. (a) Three-level DC–DC converter topology operating in buck mode. (b) Traditional TCM. (c) Proposed novel trapezoidal current mode (TZCM) to reduce the inductor peak current in near-CRM.

realize ZVS while reducing the inductor peak current, some methods have been studied recently in two-level dc–dc converters. For example, a generic ZVS scheme in parallel power MOSFETs is proposed in [21] to reduce the peak current of each switch, but it needs two parallel switches that are alternately used to conduct the rated current. The quadrilateral current modes are proposed and optimized in [22], [23], [24], and [25] for four-switch buck-boost converters to lower the inductor current ripple and rms values. However, these previous methods are mainly studied for four-switch buck-boost converters, which are not applicable to the three-level dc–dc converter.

To realize ZVS in near-CRM while reducing the inductor peak current, this article proposes a novel TZCM for three-level dc–dc converters. It not only reduces the switching losses by operating all switches in ZVS but also reduces the conduction losses of power devices by lowering the inductor current peak and rms values. A variable switching frequency control is also proposed to operate the converter under near-CRM and to realize all switches in ZVS. Compared with the previous literature, there are huge differences in inductor current shape as shown in Fig. 1, working principle, and control method.

The rest of this article is organized as follows. The detailed modulation principle, circuit modes, and comparison are analyzed in Section II. Then, a variable switching frequency control is proposed in Section III, and the comparison is described in Section IV. Finally, the proposed TZCM and control method are verified in a 2-kW three-level dc–dc converter in Section V. Finally, Section VI concludes this article.

II. Proposed TZCM to Realize ZVS in Near-CRM

The three-level dc–dc converter, illustrated in Fig. 1(a), traditionally operates in CCM, resulting in severe switching losses due to hard-switching. To mitigate these losses, the converter can be designed and controlled in either TCM or near-CRM to achieve ZVS for all four switches. In the traditional TCM, depicted in Fig. 1(b), the peak current of the inductor exceeds twice the average current. Although achieving ZVS can reduce turn-ON losses, the substantial peak current leads to significant turn-OFF current and turn-OFF losses in power semiconductor devices.

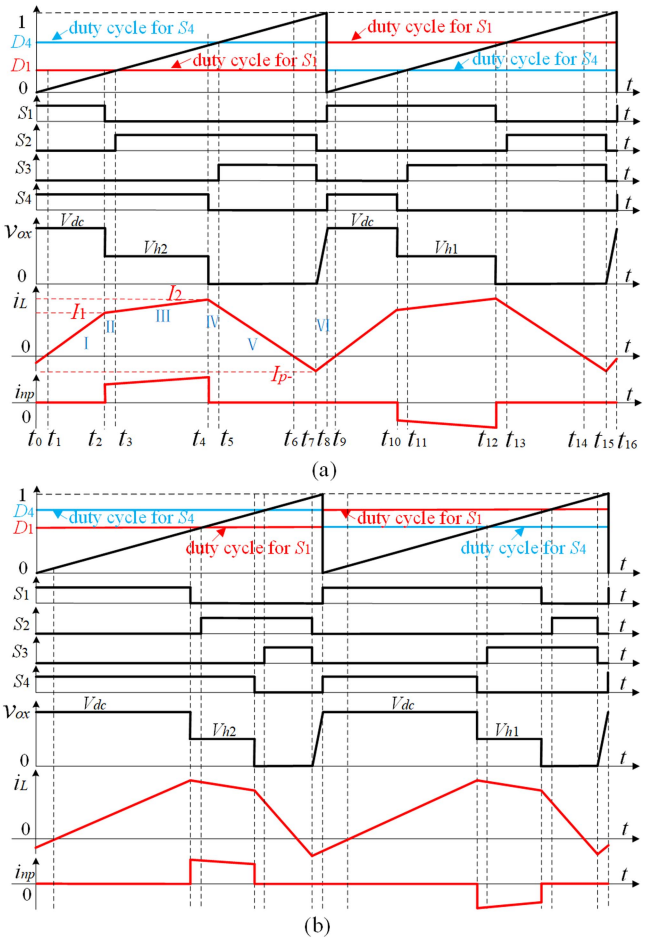

Fig. 2. Trapezoidal modulation with duty cycle swapping, which is proposed to make the three-level DC–DC converter generate trapezoidal inductor current in near-CRM with (a) $0 < D_1 + D_4 \leq 1$ and (b) $1 < D_1 + D_4 < 2$.

A. Proposed TZCM

To address the drawbacks associated with large peak currents in TCM, this article proposes a TZCM, as shown in Fig. 1(c), where the inductor current is trapezoidal or quadrilateral (nonstandard trapezoidal shape). The output sequence of the modulation adopts a 2-1-0 level, producing an approximate trapezoidal waveform for the inductor current. This technique offers significant benefits in lowering both the peak and rms currents of the inductor compared to the traditional TCM.

To realize the trapezoidal inductor current, a trapezoidal modulation principle is illustrated in Fig. 2, where S_1 and S_4 can be considered as the main switches. These switches are organized into two sets of complementary pairs, namely S_1 and S_2, S_3 and S_4. The primary operational waveforms involve two duty cycles, D_1 and D_4, which interchangeably govern the operation of S_1 and S_4. During the first switching period (odd period), D_1 and D_4 control the operation of S_1 and S_4, respectively. At the beginning of each switching cycle, the main switches S_1 and S_4 turn ON. They do not turn OFF until the carrier signals exceed the reference duty cycle values. In the subsequent switching period (even period), D_1 and D_4 are exchanged with each other, directing their operation to S_4 and S_1, respectively.

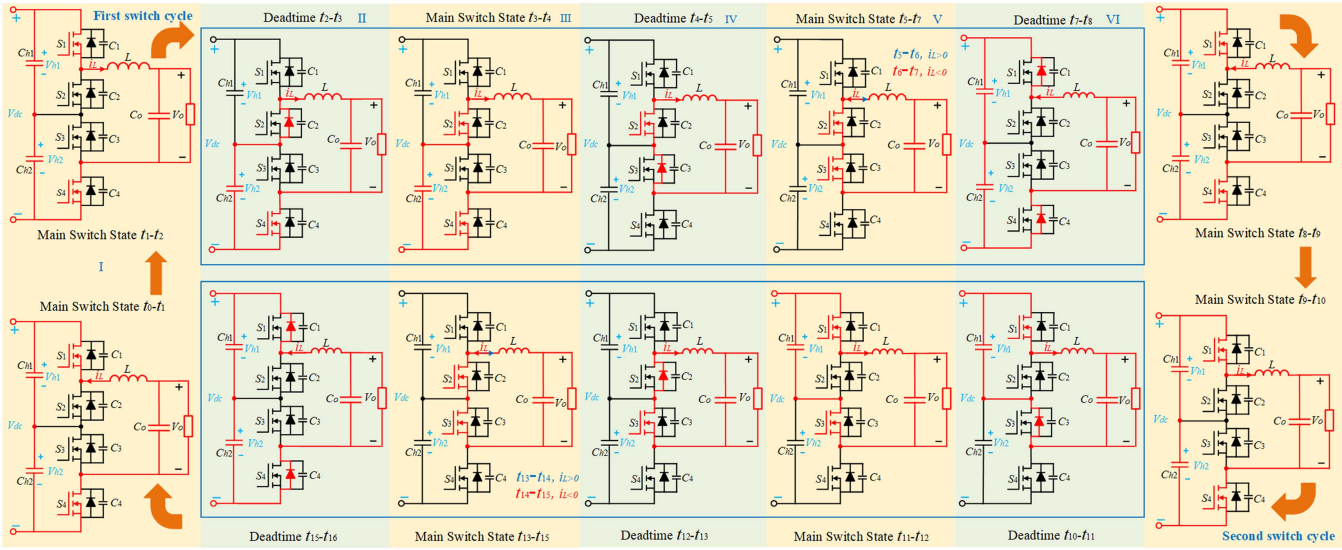

Fig. 3. Switching mode equivalent circuit diagrams of the trapezoidal modulation for the three-level DC–DC converter in TZCM.

For the proposed TZCM in the three-level dc–dc converter, the output switching voltage v_{ox} changes from V_{dc}-V_{h2}-0 in the odd period to V_{dc}-V_{h1}-0 in the even period. Consequently, the inductor current waveforms are divided into three linear segments. Moreover, the duty cycles of S_1 and S_4 are interchanged in each period to promote voltage balancing across the two series capacitors C_{h1} and C_{h2}. In accordance with the volt-second balance and the superposition principle, the average voltage during the first switching period is

$$V_{o1} = D_1 V_{h1} + D_4 V_{h2}. \tag{1}$$

The average voltage during the second switching period is

$$V_{o2} = D_1 V_{h2} + D_4 V_{h1}. \tag{2}$$

By solving for the average over two periods, the final output voltage can be Forted as

$$\begin{aligned} V_o &= \frac{1}{2}\left(V_{o1} + V_{o2}\right) = \frac{D_1 + D_4}{2}\left(V_{h1} + V_{h2}\right) \\ &= \frac{D_1 + D_4}{2} V_{\mathrm{dc}} = D V_{\mathrm{dc}}. \end{aligned} \tag{3}$$

Considering the deadtime and the positive/negative inductor currents, the trapezoidal modulation waveforms are divided into 16 intervals from t_0 to t_{16} as shown in Fig. 2(a), and their corresponding switching mode equivalent circuit diagrams are presented in Fig. 3.

Taking the first switching cycle as an example, from t_0 to t_1, S_1 and S_4 conduct the inductor current inversely for a short time. Then, from t_1 to t_2, S_1 and S_4 conduct positively until the inductor current rises linearly to the first peak current I_1 at t_2.

During the intervals t_0–t_1 and t_1–t_2, while neglecting voltage drops in power switch devices, the slope of the inductor current is

$$\frac{di_L}{dt} = \frac{V_{\mathrm{dc}} - V_o}{L}. \tag{4}$$

During the interval t_2–t_3, the inductor current flows the body diode of S_2. From t_3 to t_4, S_2 and S_4 negatively conduct the inductor current. Neglecting voltage drops in power switch devices, the slope of inductor current during the intervals t_2–t_3 and t_3–t_4 is

$$\frac{di_L}{dt} = \frac{V_{h2} - V_o}{L}. \tag{5}$$

During the intervals t_4–t_5, t_5–t_6, and t_6–t_7, the inductor current drops to a negative value, and its slope is

$$\frac{di_L}{dt} = \frac{-V_o}{L}. \tag{6}$$

The second switching cycle follows a similar pattern to the first one, except that the switching states during the second linear inductor current segment are different. In this process, S_1 and S_3 are turned ON, the slope of the inductor current is

$$\frac{di_L}{dt} = \frac{V_{h1} - V_o}{L}. \tag{7}$$

To facilitate the voltage balancing of the two series capacitors, the duty cycle D_1 and D_4 are assigned alternately to the main switch S_1 and S_4 during the odd and even periods. In order to simplify the analysis, the smaller duty cycle is assigned to D_1 and the larger duty cycle is assigned to D_4 so that only the case $0<D_1<D_4<1$ is analyzed. In addition, the two series capacitor voltages are well balanced, i.e., $V_{h1} = V_{h2} = 0.5V_{dc}$. The change of the inductor current during the first linear segment, ranging from t_0 to t_2, can be solved as

$$\Delta i_{L1} = \frac{V_{\mathrm{dc}} - V_o}{L f_{\mathrm{sw}}} D_1. \tag{8}$$

The change of the inductor current during the third linear segment, ranging from t_4 to t_7, can be solved as

$$\Delta i_{L2} = \frac{V_o}{L f_{\mathrm{sw}}}\left(1 - D_4\right). \tag{9}$$

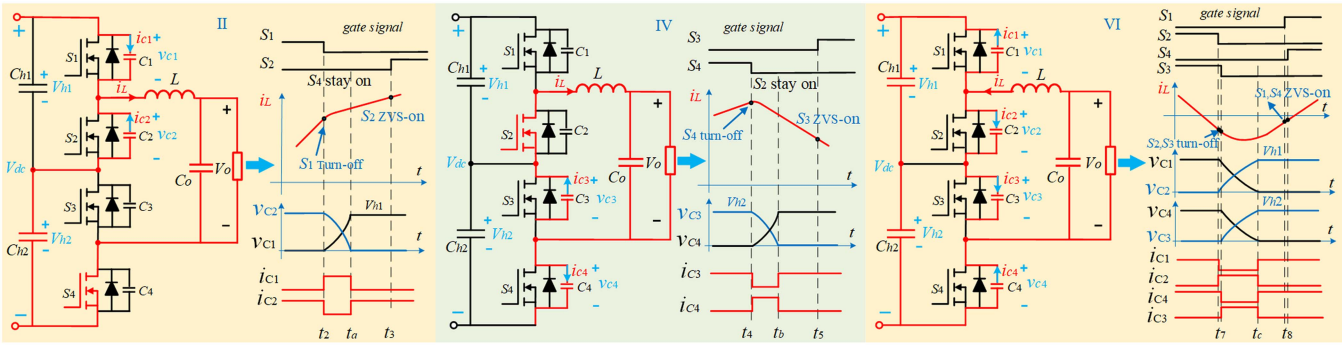

Fig. 4. Equivalent resonant transition states at (a) first peak current I_1, (b) second peak current I_2, and (c) valley current I_{p-}.

By solving the area of the trapezoidal current, the average inductor current I_{Lavg} can be expressed as

$$I_{Lavg} = \frac{1}{2}\left[D_1\Delta i_{L1} + (D_4 - D_1)(\Delta i_{L1} + \Delta i_{L2}) + (1 - D_4)\Delta i_{L2}\right] - |I_{p-}|. \quad (10)$$

By substituting (3), (8), and (9) into (10), the average inductor current can be solved as

$$I_{Lavg} = \frac{\left(D_1 + D_4 - {D_1}^2 - {D_4}^2\right)V_{dc}}{4Lf_{sw}} - |I_{p-}| \quad (11)$$

where I_{p-} is a negative valley current and f_{sw} is the switching frequency.

The three linear inductor current segments construct the trapezoidal current waveform. At the turning points of these linear segments, resonant transitions occur, which are the key to realizing ZVS.

B. ZVS Transition in Near-CRM

With the trapezoidal modulation and proper control, the three-level dc–dc converter can work in TZCM with near-CRM, enabling ZVS soft-switching for all four switches. There are three resonant transition zones at (a) the first peak current I_1; (b) the second peak current I_2; and (c) the valley current I_{p-}, as shown in Fig. 4.

At the first peak current I_1, as shown in Fig. 4(a), the resonance process is triggered by the turn-OFF action of S_1. Then, the resonance between the inductor L and the parasitic capacitors C_1 and C_2 is generated until the voltage v_{C2} is clamped by the body diode of S_2. At the end of the deadtime, a high level is applied to the gate signal of S_2, while the voltage v_{C2} is close to zero due to the inductor current flowing through the body diode of S_2, so S_2 is turned ON with ZVS.

When S_4 is turned OFF at the second peak current I_2, as shown in Fig. 4(b), a resonant network is established between the inductor L and the parasitic capacitors C_3 and C_4. Within the resonance interval t_4–t_b, C_4 is charged to V_{h2}, while C_3 is discharged to 0 until v_{C3} is clamped by the body diode of S_3. Consequently, S_3 realizes ZVS turn-ON naturally.

During the negative valley current, S_2 and S_3 are nearly turned OFF simultaneously so that a resonance network among L, C_1, C_2, C_3, and C_4 is formed. During the course of the resonance transition, C_2 and C_3 are charged to V_{h1} and V_{h2}, respectively, whereas C_1 and C_4 are discharged to 0. When the inductor current flows the body diodes of S_1 and S_4, i.e., the inductor current at t_8 is less than 0, both S_1 and S_4 naturally realize ZVS turn-ON.

From the abovementioned analysis of the resonant process, it is evident that a crucial condition for the four switches to achieve ZVS is that the inductor current must encompass both positive and negative values throughout each switching cycle. To reduce the conduction loss and turn-OFF loss, a small negative inductor current should be adopted. However, the negative inductor current cannot be too small to lose the ZVS process. According to [1], [5], and [7], to realize the ZVS, the valley current at the turn-OFF moment must satisfy

$$|I_{p-}| > \sqrt{Q_{oss,equ}\left(V_{dc} - 4V_o\right)/L} \approx \sqrt{0.5V_{dc}C\left(V_{dc} - 4V_o\right)/L} \quad (12)$$

where C represents the charge-equivalent capacitance from 0 to $0.5V_{dc}$ for the nonlinear parasitic capacitor of the switch device [7]. For example, $C = 236$ pF for SiC C3M0025065K. Using (12), the negative valley current can be calculated as $I_{p-} < -0.55$ A with $V_{dc} = 600$ V and $L = 140$ μH. In the experiment below, I_{p-} is chosen as -1 A. Referring to [5] and [19], the deadtime for the three-level dc–dc converter can be designed as 0.5 μs when $I_{p-} = -1$ A.

III. Proposed Variable Switching Frequency Control

In order to make the three-level dc–dc converter operate in near-CRM, the converter can be controlled with proper inductor current ripple by adjusting the switching frequency [6], [26]. Based on (11), the switching frequency can be expressed as

$$f_{sw} = \frac{\left(D_1 + D_4 - {D_1}^2 - {D_4}^2\right)V_{dc}}{4\left(I_{Lavg} + |I_{p-}|\right)L} \quad (13)$$

where I_{p-} is a constant set to the appropriate value based on (12), D_1 and D_4 are subject to two side constraints. One is that the sum of D_1 and D_4 must satisfy

$$D_1 + D_4 = \frac{2V_o}{V_{dc}}. \quad (14)$$

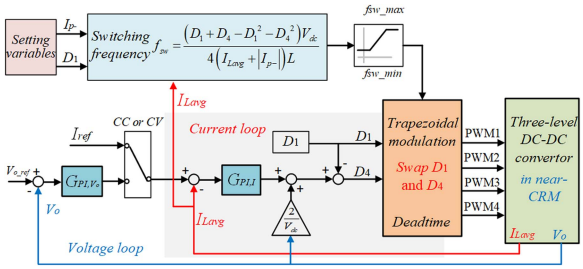

Fig. 5. Proposed TZCM-based variable switching frequency control to make the three-level DC–DC operate in near-CRM with reduced peak and rms currents.

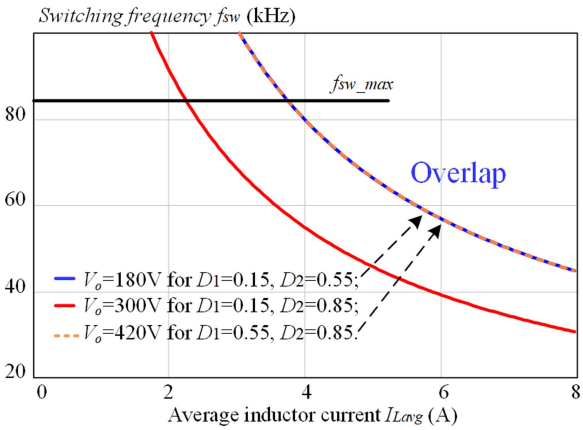

Fig. 6. Relationship between the switching frequency and the average inductor current with $V_{\rm dc} = 600$ V, $I_{p\text{-}} = -1$ A, and $L = 140$ μH.

The other is that the peak and rms currents of the inductor and power switches should be small so that the converter has better efficiency. Based on the comparison in Section IV, D_1 can be selected as 0.1–0.2 to get relatively small peak and rms currents.

By introducing the required switching frequency into the control system, the proposed TZCM-based variable switching frequency control for the three-level dc–dc converter is shown in Fig. 5, which is operated in near-CRM with reduced peak current. The variable $I_{p\text{-}}$ is set based on (12), and D_1 can be designed based on the comparison in Section IV, where D_1 is chosen to be 0.15 to keep the peak and rms currents small.

Based on (13), the inductor value can be expressed as

$$L = \frac{\left(D_1 + D_4 - {D_1}^2 - {D_4}^2\right) V_{\rm dc}}{4\left(I_{L\rm avg} + |I_{p-}|\right) f_{\rm sw}}. \tag{15}$$

Designing the inductor value needs some careful considerations, including the switching frequency range, the valley current value, the output current, and the nonlinear characteristics [27]. Take a battery charging application as an example: $V_{dc} = 600$ V, $V_o = 200$–400 V, $f_{sw} = 20$–60 kHz, and $I_{L\rm avg} = 0$–8 A. The inductance can be calculated to be a maximum of 150 μH at the operating limit with a minimum switching frequency of 20 kHz, a minimum $D_1 = 0.1$, and a maximum output current of 8 A. Considering some margin for the switching frequency, the inductance can be selected as 140 μH. The relationship between the switching frequency and the average inductor current is shown in Fig. 6. As the average inductor current (equal to the output load current) increases, the switching frequency decreases.

IV. Comparison With Traditional Triangular Modulation

A. Peak and RMS Current of the Inductor

By combining (8), (9), and (13), the two peak values of the trapezoidal inductor current can be expressed as

$$\begin{cases} I_1 = \Delta i_{L1} - |I_{p-}| = \frac{4(I_{L\rm avg}+|I_{p-}|)(V_{\rm dc}-V_o)D_1}{\left(D_1+D_4-{D_1}^2-{D_4}^2\right)V_{\rm dc}} - |I_{p-}| \\ I_2 = \Delta i_{L2} - |I_{p-}| = \frac{4(I_{L\rm avg}+|I_{p-}|)V_o(1-D_4)}{\left(D_1+D_4-{D_1}^2-{D_4}^2\right)V_{\rm dc}} - |I_{p-}| \end{cases} \tag{16}$$

where I_1 is the first peak current, I_2 is the second peak current, and $I_{p\text{-}}$ is the valley current that is set based on (12).

The maximum peak current is

$$i_{L\rm peak} = \max\{I_1, I_2\}. \tag{17}$$

Using the superposition principle for the three linear segments, the inductor rms current can be calculated as (18) shown at the bottom of the next page.

Compared to the traditional modulation, the proposed new modulation method not only realizes ZVS soft-switching in near-CRM but also has smaller inductor peak and rms currents, as shown in Fig. 7. It is evident that the smaller the duty cycle D_1, the lower both the inductor's peak current and rms current. This is advantageous for mitigating conduction losses and turn-OFF losses in power semiconductor switches. However, the reduction of duty cycle D_1 is limited by factors such as output voltage, input voltage, average inductor current, negative current, switching frequency, and inductor value. Consequently, there exists a minimum peak current point during the reduction of duty cycle D_1. When D_1 falls below the value corresponding to the minimum peak current point, the switching peak current increases instead of decreasing, as shown in Fig. 7(a).

B. Peak and RMS Current of the Switch Devices

The current waveforms of the power devices using the traditional modulation and the proposed trapezoidal modulation are shown in Fig. 8. Using the traditional modulation at $D \neq 0.5$, the inductor current ripple is sufficient around $D = 0.25$ or 0.75. But when $D = 0.5$ ($D = V_o/V_{\rm dc} = 0.5$) for the triangular modulation, the inductor current ripple is almost zero, and fails to operate the converter in near-CRM. Therefore, the traditional modulation cannot realize ZVS in the full working range, which must be considered to move away from the working point at $D = 0.5$.

However, for the proposed trapezoidal modulation, the current ripple is still sufficient to be in near-CRM at $D = 0.5$, as shown in Fig. 8(c). It has sufficient inductor current ripple over a wide range of duty cycles to work in near-CRM.

By analyzing the peak and rms current waveforms of the inductor and the switches, as shown in Fig. 8, and combining expressions (16) and (17), the peak currents of the switches can be obtained as

$$i_{S\rm peak} = i_{L\rm peak} = \max\{I_1, I_2\} \tag{19}$$

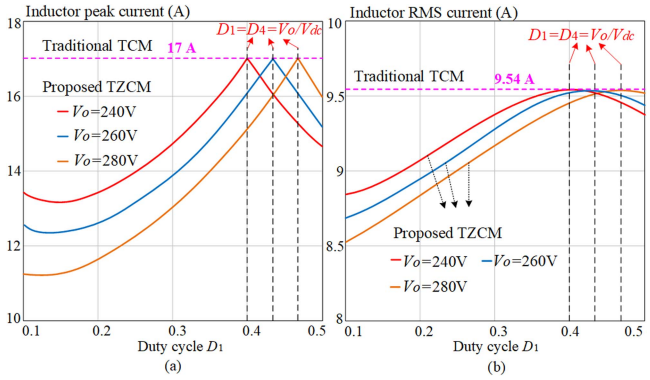

Fig. 7. Comparison of (a) the inductor peak current and (b) the inductor rms current between proposed TZCM and traditional TCM, with $V_{\rm dc} = 600$ V, $I_{Lavg} = 8$ A, and $I_{p-} = -1$ A.

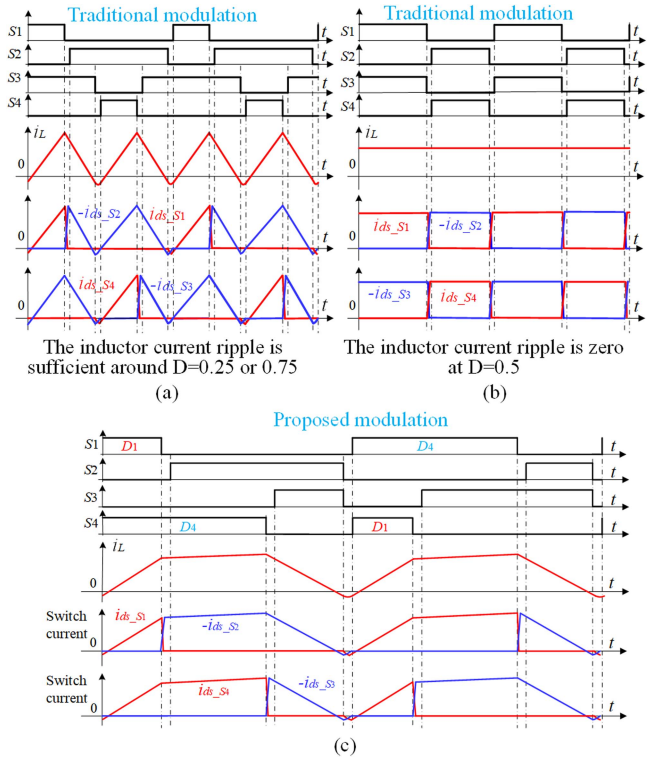

Fig. 8. Comparison of current waveforms under different modulations for TCM and TZCM. (a) Traditional modulation with $D \neq 0.5$, where the inductor current ripple is sufficient around $D = 0.25$ or 0.75. (b) Traditional modulation in [2] and [4] with $D = 0.5$, where the inductor current ripple is almost zero around $D = 0.5$, and does not work in near-CRM. (c) Proposed trapezoidal modulation, which has sufficient current ripple over a wide range of duty cycles.

and the rms currents of the switches can be obtained as

$$I_{S_1,S_4\_\rm rms} = \sqrt{\frac{{I_1}^2+I_1I_{p-}+{I_{p-}}^2}{3}D_1 + \frac{{I_1}^2+I_1I_2+{I_2}^2}{6}(D_4-D_1)} \tag{20}$$

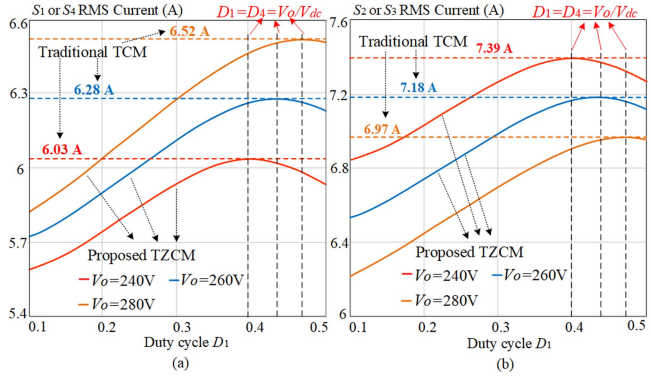

Fig. 9. Comparison of the rms currents of the switch devices under different modes with $V_{\rm dc} = 600$ V, $I_{Lavg} = 8$ A and $I_{p-} = -1$ A. (a) RMS current of switch S_1 or S_4. (b) RMS current of switch S_2 or S_3.

$$I_{S_2,S_3\_\rm rms} = \sqrt{\frac{{I_1}^2+I_1I_2+{I_2}^2}{6}(D_4-D_1) + \frac{{I_2}^2+I_2I_{p-}+{I_{p-}}^2}{3}(1-D_4)} \tag{21}$$

where $i_{S\rm peak}$ represents the peak current of all four switches, $I_{S1,S4\_\rm rms}$ represents the rms current of S_1 and S_4, and $I_{S2,S3\_\rm rms}$ represents the rms current of S_2 and S_3.

According to (19) and Fig. 7(a), the peak currents of the four switches are equal to the peak current of the inductor, so it can be directly concluded that the TZCM proposed in this article has the smaller peak currents for the four switches compared to the traditional TCM.

The rms currents of the switch devices under different modes are shown in Fig. 9. It can be observed that, as the duty cycle decreases, the rms currents of the four switches gradually decrease. In addition, for $D_1 + D_4 < 1$ (i.e., $V_o < 300$ V), where the conduction duration of switches S_2 and S_3 are longer than that of switches S_1 and S_4, the rms current of S_2 and S_3 is greater than that of S_1 and S_4. In any case, the rms current of the proposed TZCM is smaller than that of the traditional TCM, which indicates that the conduction losses of the power switches can be reduced in TZCM.

C. RMS Ripple Current of the Input/Output Capacitor

The input and output ripple currents are absorbed by the input filter capacitors C_{h1}, C_{h2}, and the output filter capacitor C_o, respectively. By combining (11) and (20), the rms current of C_{h1} and C_{h2} can be obtained as

$$I_{C_{h1},C_{h2}\_\rm rms} = \sqrt{{I_{S_1,S_4\_\rm rms}}^2 - D^2{I_{Lavg}}^2}. \tag{22}$$

$$I_{L\rm rms} = \sqrt{\frac{{I_1}^2+I_1I_{p-}+{I_{p-}}^2}{3}D_1 + \frac{{I_1}^2+I_1I_2+{I_2}^2}{3}(D_4-D_1) + \frac{{I_2}^2+I_2I_{p-}+{I_{p-}}^2}{3}(1-D_4)}. \tag{18}$$

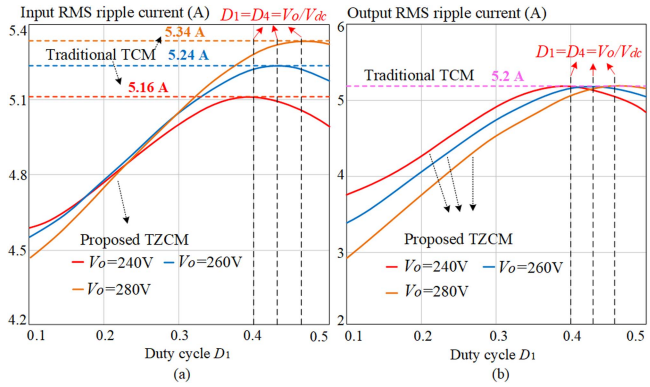

Fig. 10. Comparison of input/output rms ripple currents under different modes with $V_{\rm dc} = 600$ V, $I_{L\rm avg} = 8$ A, and $I_{p\text{-}} = -1$ A. (a) Input rms ripple current absorbed by C_{h1} and C_{h2}. (b) Output rms ripple current absorbed by C_o.

By combining (11) and (21), the rms current of C_o can be obtained as

$$I_{C_o\_\rm rms} = \sqrt{{I_{L\rm rms}}^2 - {I_{L\rm avg}}^2}. \tag{23}$$

The comparison of input/output rms current ripple under different modes is shown in Fig. 10, where the proposed TZCM has smaller rms ripple currents. As the duty cycle D_1 decreases, the rms ripple currents for both the input and output capacitors also decrease.

Therefore, compared to the traditional TCM, the proposed TZCM in this article not only has smaller peak and rms currents for both the inductor and the four switches but also has smaller rms ripple currents of the input and output capacitors. As a result, the peak and rms currents for the inductor, the four switches and the input/output capacitors are reduced, which is beneficial for improving the efficiency of the three-level dc–dc converter.

D. Power Loss Evaluation

To evaluate the power loss of the three-level dc–dc converter operated in TZCM, the conduction and switching losses of the power device are calculated. Based on Fig. 8(c), the inductor current always flows through two complementary switches in four main switches, so the conduction loss can be calculated as

$$P_{\rm Cond} = 2I_{L\rm rms}^2 R_{\rm DSon}. \tag{24}$$

Because all four switches realize ZVS turn-ON, there are no turn-ON losses of switch devices and reverse recovery losses of body diodes. Based on Fig. 8(c) and [5], the switching losses are

$$P_{\rm sw1} = P_{\rm sw4} = 0.5 f_{\rm sw} \left(E_{{\rm off},I_1} + E_{{\rm off},I_2}\right) \tag{25}$$

$$P_{\rm sw2} = P_{\rm sw3} = f_{\rm sw} E_{{\rm off},I_{p\text{-}}} \tag{26}$$

where $E_{{\rm off},I1}$ is the turn-OFF energy at I_1, $E_{{\rm off},I2}$ is the turn-OFF energy at I_2, and $E_{{\rm off},Ip\text{-}}$ is the turn-OFF energy at $I_{p\text{-}}$, which can be found in the manufacturer's datasheet or measured by double pulse test.

Referring to [5] and [28], the copper loss of the inductor mainly consists of dc resistance and high-frequency ac resistance, which is calculated as

$$P_{\rm Copper} = I_{L\rm rms,dc}^2 R_{\rm dc} + I_{L\rm rms,ac}^2 R_{\rm ac}. \tag{27}$$

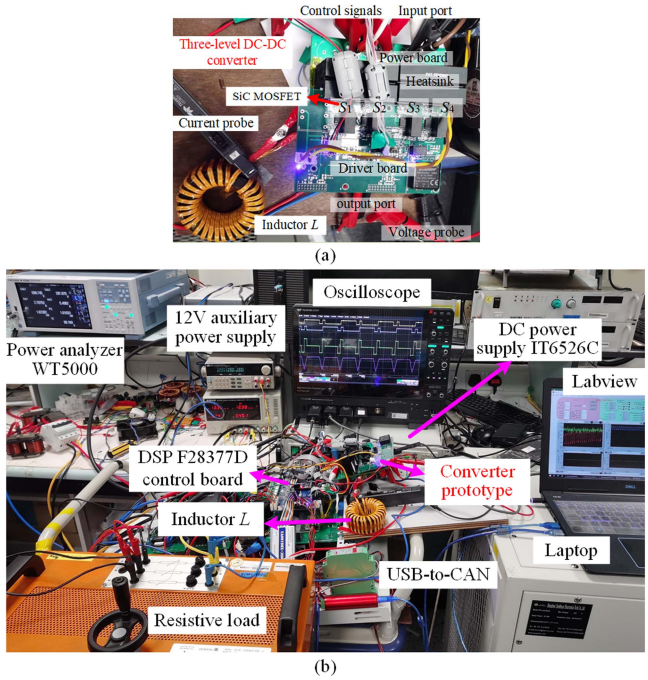

Fig. 11. (a) Experimental prototype of the three-level DC–DC converter. (b) Experimental test setup platform.

And the core loss of the inductor is calculated as

$$P_{\rm Core} = \alpha f_{\rm sw}^{\beta} \left(\frac{L\Delta I_L}{2NA_e}\right)^{\gamma} V_e \tag{28}$$

where V_e is the volume of the magnetic core, A_e is the effective cross-section area, and α, β, γ are the core material loss coefficients, which can be found in the magnetic core manufacturer's datasheet.

The input/output capacitor losses caused by the rms ripple currents are calculated as

$$P_{C_{h1},C_{h2}} = 2I_{C_{h1},C_{h2}\_\rm rms}^2 R_{C_{h1},C_{h2}} \tag{29}$$

$$P_{C_o} = I_{C_o\_\rm rms}^2 R_{C_o} \tag{30}$$

where $R_{Ch1,Ch2}$, and R_{Co} are the high-frequency equivalent resistances of the input and output capacitors, respectively.

V. Experimental Results

To verify the proposed trapezoidal modulation scheme, a three-level dc–dc converter prototype is built as shown in Fig. 11. The type of power switch is SiC MOSFET C3M0025065K, the controller is DSP F28377D, and an inductance of 140 μH is selected to operate the switching frequency in the range of 20–60 kHz. The input and output electrolytic capacitors are 330 μF and 440 μF. The inductor is wound using two KS301026 magnetic cores and 29 turns of Litz wire.

The waveforms of the proposed trapezoidal modulation under different duty cycles at 50 kHz are shown in Fig. 12. These inductor currents are in near-CRM with a negative valley current. When the sum of D_1 and D_4 is close to 1, the inductor current waveform is almost a standard trapezoidal shape. It can be seen

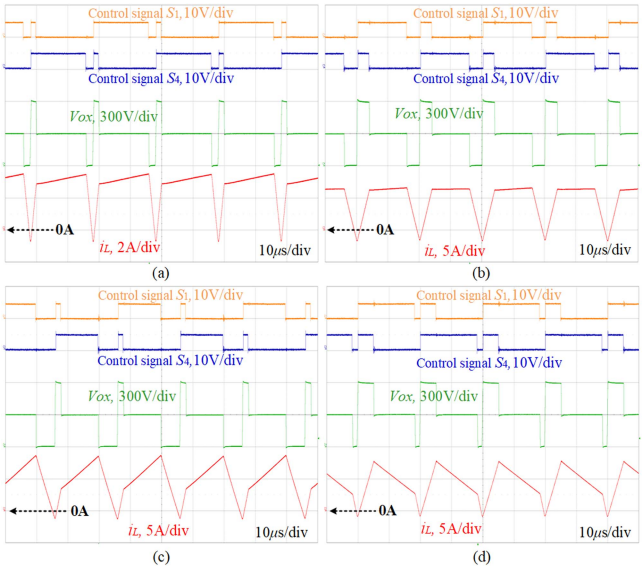

Fig. 12. Waveforms of the proposed TZCM at different duty cycles with f_{sw} = 50 kHz and deadtime = 0.5 μs. (a) $D_1 = 0.1$ and $D_4 = 0.9$. (b) $D_1 = 0.2$ and $D_4 = 0.8$. (c) $D_1 = 0.1$ and $D_4 = 0.7$. (b) $D_1 = 0.27$ and $D_4 = 0.93$.

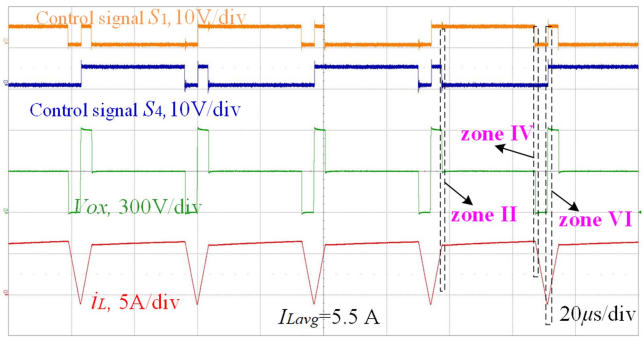

Fig. 13. Waveforms of the proposed TZCM with 1.6 kW output power at D_1 = 0.15, $D_4 = 0.85$, and $V_{\rm dc} = 600$ V, $V_o = 296$ V.

that the inductor current with three different slopes is caused by three different v_{ox} voltage levels 2-1-0, i.e., 600V-300V-0.

Fig. 13 shows the test waveforms of the proposed TZCM with 1.6 kW output power at $D_1 = 0.15$, $D_4 = 0.85$, and $V_{\rm dc} = 600$ V. Theoretically, the output voltage is 300 V, but due to the effect of dead time, the actual output voltage is 296 V. The average current of the inductor is 5.5 A, but the peak current is only 6.4 A and the rms current is only 5.8 A, which are less than that of the traditional TCM.

The ZVS transition waveforms of Fig. 13 in near-CRM with the proposed TZCM are magnified as shown in Fig. 14. There are three ZVS regions: around the negative valley current $I_{p\text{-}}$, around the first peak current I_1, and around the second peak current I_2. Around the negative valley current, S_1 and S_4 realize ZVS turn-ON as long as the inductor current at the turn-ON moment is less than zero. While S_2 and S_3 still turn ON with ZVS in both CCM and near-CRM because the positive inductor current flows through the body diodes of S_2 and S_3 at the moment to turn them ON.

Based on the proposed control in Fig. 5, the dynamic waveforms as the output current changes from 5 to 2 A are shown in

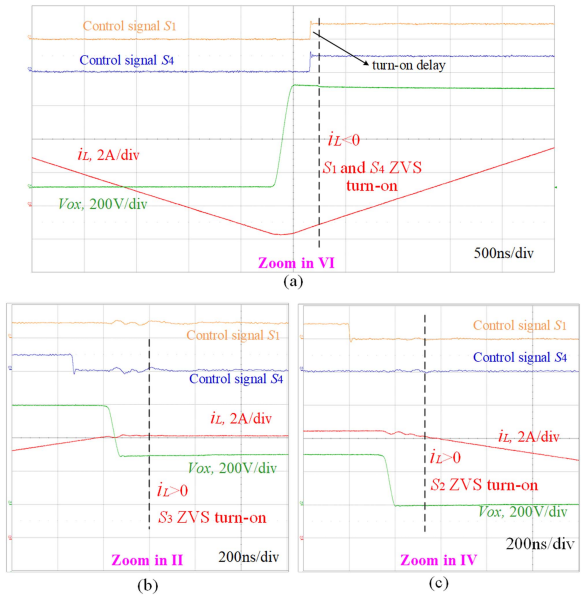

Fig. 14. ZVS transition waveforms zooming in Fig. 13(b) in near-CRM with new modulation. (a) Around the valley current $I_{p\text{-}}$. (b) Around the first peak current I_1. (c) Around the second peak current I_2.

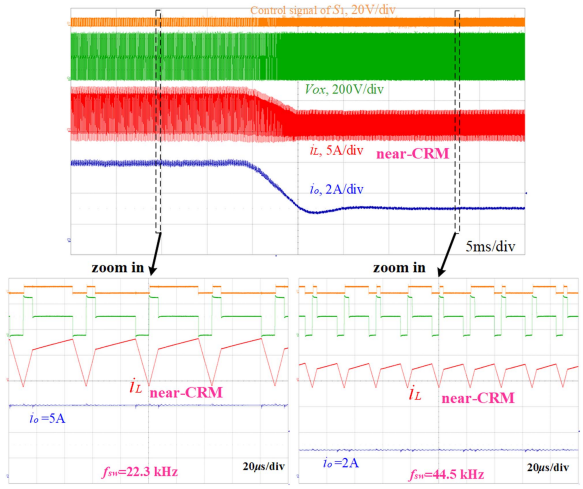

Fig. 15. Dynamic test waveforms when output current changes from 5 to 2 A, where the output port is a voltage source such as a battery.

Fig. 15. It verifies that the three-level dc–dc converter still works in near-CRM with the proposed TZCM by variable switching frequency control. As the output current goes down from 5 to 2 A, the switching frequency increases from 22.3 to 44.5 kHz.

As shown in Fig. 16, the dynamic tests when the output voltage changes from 120 to 200 V are to verify the proposed modulation and control method in near-CRM for this converter. It is implemented by relying on the control diagram in Fig. 5 with an output voltage loop. During the voltage changes, the inductor current is still trapezoidal and in near-CRM. Since the output capacitor is present, the change of V_o will generate some currents to charge/discharge the capacitor C_o.

The experimental waveforms of the startup process for the three-level dc–dc converter are divided into two operating modes: one is that the output port is a voltage source, such as a

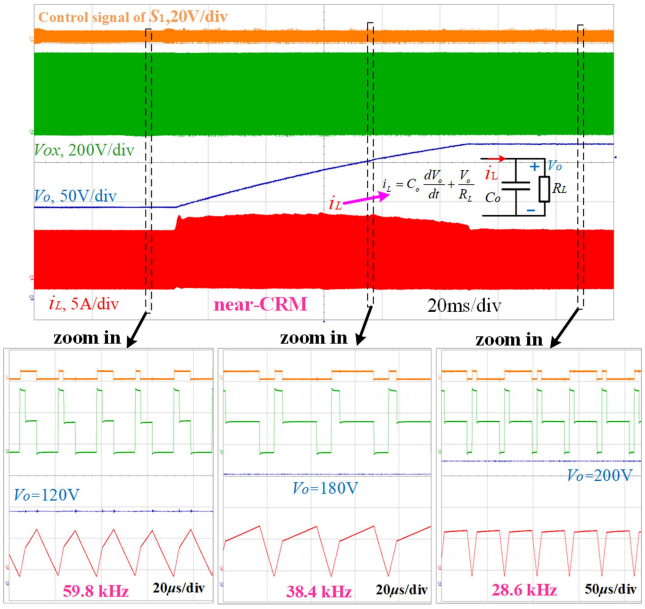

Fig. 16. Dynamic test waveforms when output voltage changes from 120 to 200 V, where the output port is a resistor load.

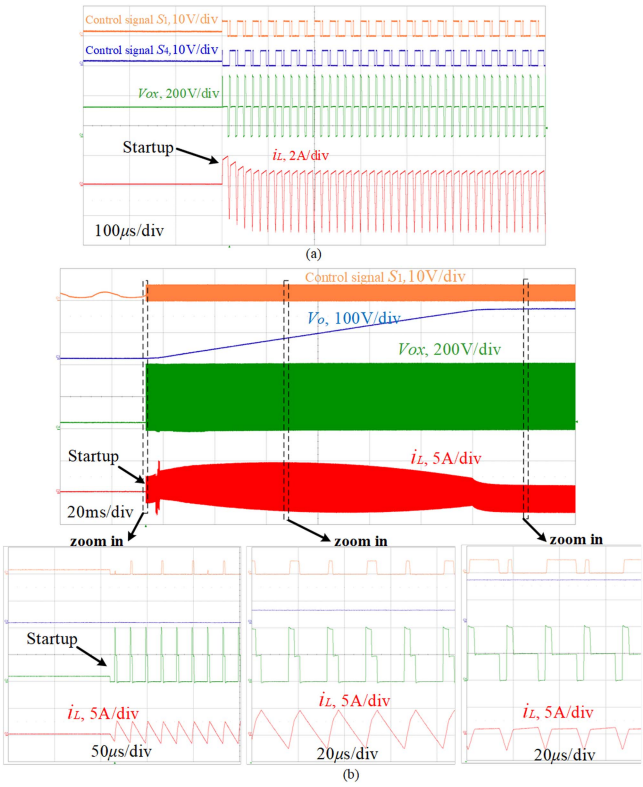

Fig. 17. Waveforms of the converter startup process. (a) Output port is a voltage source, such as a battery. (b) Output port is a resistor load.

battery, where the startup is relatively easy and the steady state can be reached quickly, as shown in Fig. 17(a). The other is that the output port is a resistive load, but the startup will be slower due to the output filter capacitor that needs to be charged, as shown in Fig. 17(b).

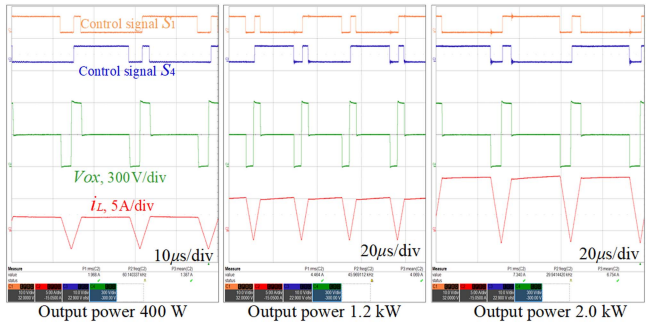

Fig. 18. Steady state waveforms at 400 W, 1.2 kW, and 2.0 kW output power with $V_{\rm dc} = 600$ V and $V_o = 296$ V.

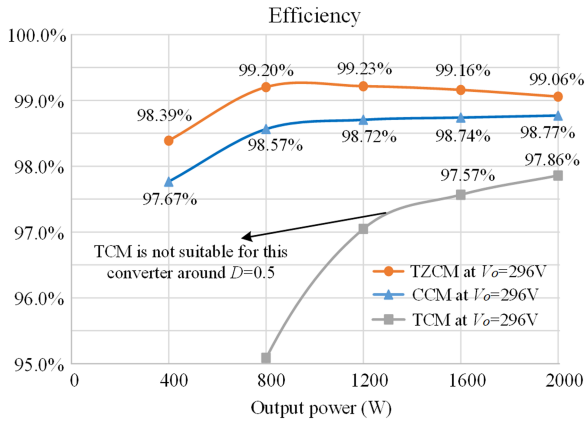

Fig. 19. Efficiency results of the proposed TZCM and the traditional operation modes for the three-level DC–DC converter with the same hardware prototype at $V_{\rm dc} = 600$ V.

Fig. 18 shows the steady state waveforms at 400 W, 1.2 kW, and 2.0 kW output power with $V_{\rm dc} = 600$ V and $V_o = 296$ V. At light loads such as 400 W, the negative peak current is a somewhat large due to the maximum switching frequency limit of 60 kHz. As the output power increases, the required switching frequency is reduced to realize variable switching frequency control, so the converter works in near-CRM with a smaller negative peak current.

The efficiency of the proposed TZCM and control method for the three-level dc–dc converter at $V_{\rm dc} = 600$ V, $V_o = 296$ V is shown in Fig. 19, which reaches 99.06% efficiency at 2 kW.

In order to compare the efficiency in TCM, we operate this converter with two-level modulation to produce enough inductor current ripple. Although the TCM can be achieved with two-level modulation (TCM cannot be achieved with conventional three-level modulation at $D = 0.5$), the efficiency of the converter is lower than that of TZCM and CCM due to the large inductor current ripple caused by the two-level modulation. In fact, TCM is not suitable for this three-level converter around $D = 0.5$. The proposed TZCM is most advantageous around $D = 0.5$ because the inductor current is almost a standard trapezoidal wave with a lower peak and rms inductor current for the same average current.

The loss breakdown of the three-level dc–dc converter is shown in Fig. 20(a), which is theoretically calculated. The switching losses include only turn-OFF losses, where there are

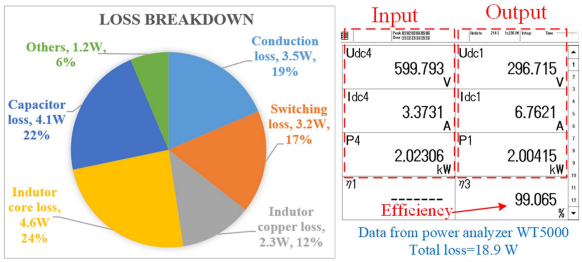

Fig. 20. (a) Loss breakdown for the 2-kW three-level DC–DC converter with 99.06% efficiency. (b) Measured data with 18.9 W loss from the power analyzer WT5000.

no turn-ON losses of switch devices and reverse recovery losses of body diodes because all four switches realize ZVS turn-ON. The largest percentage is the core loss of the inductor, which is 24%. The others mainly consist of PCB copper loss, body diode conduction loss during deadtime, and some errors. The measured data from the power analyzer WT5000 at 2 kW is shown in Fig. 20(b), which is in general agreement with the theoretical calculations.

VI. Conclusion

This article proposes a novel TZCM to reduce the inductor peak current in near-CRM for three-level dc–dc converters. Compared to the traditional TCM, the proposed mode and method in this article effectively reduces both the peak and rms current of the inductor, the four power switches, and the input/output capacitors. A variable switching frequency control is also proposed to operate the converter under near-CRM and to realize all switches in ZVS. The experiments are performed in a 2-kW three-level dc–dc converter with 99.06% efficiency, which verifies the feasibility of the proposed TZCM and control method. TZCM has the advantage of ZVS soft-switching and lower peak/rms inductor current, so the proposed method is valuable to realize the high efficiency of the three-level dc–dc converter.

References

[1] D. Chou, Y. Lei, and R. C. N. Pilawa-Podgurski, "A zero-voltage-switching, physically flexible multilevel GaN DC–DC converter," *IEEE Trans. Power Electron.*, vol. 35, no. 1, pp. 1064–1073, Jan. 2020.

[2] P. J. Grbović, P. Delarue, P. Le Moigne, and P. Bartholomeus, "A bidirectional three-level DC–DC converter for the ultracapacitor applications," *IEEE Trans. Ind. Electron.*, vol. 57, no. 10, pp. 3415–3430, Oct. 2010.

[3] S. Dusmez, A. Hasanzadeh, and A. Khaligh, "Comparative analysis of bidirectional three-level DC–DC converter for automotive applications," *IEEE Trans. Ind. Electron.*, vol. 62, no. 5, pp. 3305–3315, May 2015.

[4] L. Tan, N. Zhu, and B. Wu, "An integrated inductor for eliminating circulating current of parallel three-level DC–DC converter-based EV fast charger," *IEEE Trans. Ind. Electron.*, vol. 63, no. 3, pp. 1362–1371, Mar. 2016.

[5] Z. He et al., "Optimized modulation method for three-level boost converter with ZVS under unbalanced-load operation," *IEEE Trans. Power Electron.*, vol. 38, no. 11, pp. 13811–13824, Nov. 2023.

[6] Z. Yao and S. Lu, "Voltage self-balance mechanism based on zero-voltage switching for three-level DC–DC converter," *IEEE Trans. Power Electron.*, vol. 35, no. 10, pp. 10078–10087, Oct. 2020.

[7] M. Kasper, R. Burkart, G. Deboy, and J. W. Kolar, "ZVS of power MOSFETs revisited," *IEEE Trans. Power Electron.*, vol. 31, no. 12, pp. 8063–8067, Dec. 2016.

[8] B. Hu, Y. Jiang, L. Shillaber, H. Wang, C. Li, and T. Long, "Optically triggered self-adaptive zero voltage switching," *IEEE Trans. Power Electron.*, vol. 38, no. 9, pp. 10600–10605, Sep. 2023.

[9] Y. Chen and D. Xu, "Review of soft-switching topologies for single-phase photovoltaic inverters," *IEEE Trans. Power Electron.*, vol. 37, no. 2, pp. 1926–1944, Feb. 2022.

[10] Q. Huang and A. Q. Huang, "Variable frequency average current mode control for ZVS symmetrical dual-buck H-bridge all-GaN inverter," *IEEE J. Emerg. Sel. Topics Power Electron.*, vol. 8, no. 4, pp. 4416–4427, Dec. 2020.

[11] J. Wan, F. Liu, K.-Z. Liu, and Y. Li, "An efficient soft-switching buck converter with parasitic resonance suppression in auxiliary circuit," *IEEE Trans. Ind. Electron.*, vol. 70, no. 2, pp. 1367–1377, Feb. 2023.

[12] A. Asghari, "A nonisolated soft switching interleaved converter with extended duty cycle and low output current ripple," *IEEE Trans. Ind. Electron.*, vol. 68, no. 10, pp. 9376–9385, Oct. 2021.

[13] Z. Yan, J. Zeng, Z. Guo, R. Hu, and J. Liu, "A soft-switching bidirectional DC–DC converter with high voltage gain and low voltage stress for energy storage systems," *IEEE Trans. Ind. Electron.*, vol. 68, no. 8, pp. 6871–6880, Aug. 2021.

[14] M. R. Mohammadi, B. Poorali, S. Eren, and M. Pahlevani, "A nonisolated TCM bidirectional converter with low input-current-ripple for DC microgrids," *IEEE Trans. Ind. Electron.*, vol. 68, no. 11, pp. 10845–10855, Nov. 2021.

[15] O. Knecht, D. Bortis, and J. W. Kolar, "ZVS modulation scheme for reduced complexity clamp-switch TCM DC–DC boost converter," *IEEE Trans. Power Electron.*, vol. 33, no. 5, pp. 4204–4214, May 2018.

[16] M. Haider et al., "Novel ZVS S-TCM modulation of three-phase AC/DC converters," *IEEE Open J. Power Electron.*, vol. 1, pp. 529–543, 2020.

[17] R. Kopacz, M. Harasimczuk, P. Trochimiuk, G. Wrona, and J. Rąbkowski, "Medium voltage flying capacitor DC–DC converter with high-frequency TCM-Q2L control," *IEEE Trans. Power Electron.*, vol. 37, no. 4, pp. 4233–4248, Apr. 2022.

[18] Z. Yao and S. Lu, "A simple approach to enhance the effectiveness of passive currents balancing in an interleaved multiphase bidirectional DC–DC converter," *IEEE Trans. Power Electron.*, vol. 34, no. 8, pp. 7242–7255, Aug. 2019.

[19] Z. Yao et al., "Sensorless simultaneous self-balance mechanism of voltage and current based on near-CRM in interleaved three-level DC–DC converter," *IEEE Trans. Power Electron.*, vol. 39, no. 2, pp. 2086–2099, Feb. 2024.

[20] Z. Zheng, L. Zhang, C. Wu, Y. Wang, Z. Lei, and K. Sun, "Variable off-time and deadtime scheme with optimized control frequency for soft-switching single-phase inverters," *IEEE Trans. Power Electron.*, vol. 38, no. 4, pp. 4972–4987, Apr. 2023.

[21] Y. Shen, Y. Jiang, H. Zhao, L. Shillaber, C. Jiang, and T. Long, "Quadrilateral current mode paralleling of power MOSFETs for zero-voltage switching," *IEEE Trans. Power Electron.*, vol. 36, no. 5, pp. 5997–6014, May 2021.

[22] J. Fang, X. Ruan, X. Huang, R. Dong, X. Wu, and J. Lan, "A PWM plus phase-shift control for four-switch buck-boost converter to achieve ZVS in full input voltage and load range," *IEEE Trans. Ind. Electron.*, vol. 69, no. 12, pp. 12698–12709, Dec. 2022.

[23] J. Liao, G. Qiu, Y. Huang, and V. Khadkikar, "Lagrange-multiplier-based control method to optimize efficiency for four-switch buck–boost converter over whole operating range," *IEEE Trans. Ind. Electron.*, vol. 71, no. 1, pp. 822–833, Jan. 2024.

[24] Z. Guo and T. Mao, "Efficiency optimization and control strategy of four-switch buck–boost converter for wide conversion ratio," *IEEE Trans. Power Electron.*, vol. 38, no. 9, pp. 10702–10715, Sep. 2023.

[25] G. Yu, J. Dong, T. B. Soeiro, G. Zhu, Y. Yao, and P. Bauer, "Three-mode variable-frequency ZVS modulation for four-switch buck+boost converters with ultra-high efficiency," *IEEE Trans. Power Electron.*, vol. 38, no. 4, pp. 4805–4819, Apr. 2023.

[26] S. Norouzi, H. Ghoreishy, A. Ale Ahmad, and F. Tahami, "A new variable frequency zero voltage switching control method for boost converter operating in boundary conduction mode," *Int. J. Eng.*, vol. 33, no. 11, pp. 2222–2232, Nov. 2020.

[27] Z. Yao et al., "Nonlinear inductor-based single sensor current balancing method for interleaved DC–DC converters," *IEEE Trans. Power Electron.*, vol. 39, no. 4, pp. 3996–4000, Apr. 2024.

[28] C. A. Barros et al., "Proposed inductor power loss metric and novel embedded toroidal inductor for integrated voltage regulators," *IEEE Trans. Compon., Packag. Manuf. Technol.*, vol. 11, no. 11, pp. 1935–1947, Nov. 2021.

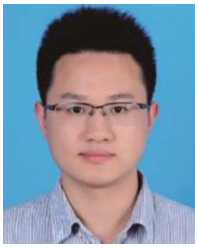

Zhigang Yao (Member, IEEE) received the B.S. and Ph.D. degrees in electrical engineering from Chongqing University, Chongqing, China, in 2014 and 2020, respectively.

In 2020, he joined the School of Electrical Engineering, Southwest Jiaotong University, Chengdu, China, as an Assistant Professor. Since September 2022, he also serves as a Research Fellow with Nanyang Technological University, Singapore. His current research interests include high power multiphase/multilevel dc–dc converters for fuel cells and batteries, LLC resonant converters, three-level grid-connected inverters, and ZVS soft-switching techniques.

Xinyu He received the B.S. degree in automation from Tianjin University of Commerce, Tianjin, China, in 2022. She is currently working toward the M.Sc. degree in electrical engineering with the School of Electrical Engineering, Southwest Jiaotong University, Chengdu, China.

Her research interests include multiphase interleaved dc–dc converters, three-level converters, and soft-switching converters.

Haogang Lan received the B.S. degree in electrical engineering and automation from Chongqing University of Technology, Chongqing, China, in 2022. He is currently working toward the M.Sc. degree in electrical engineering with the School of Electrical Engineering, Southwest Jiaotong University, Chengdu, China.

His research interests include three-level converters, bidirectional converters, and soft-switching converters.

Haoxin Yang (Member, IEEE) received the B.S. degree in electrical engineering from Wuhan University, Wuhan, China, in 2018, and the M.S. degree in power engineering in 2020 from Nanyang Technological University, Singapore, where he is currently working toward the Ph.D. degree in electrical engineering.

He is currently a Senior Research Engineer with Energy Research Institute, Nanyang Technological University, Singapore. His research interests include stability and control of distributed generations in more-electronics power systems.

Ziheng Xiao (Member, IEEE) received the B.S. and Ph.D. degrees in electrical engineering from the College of Electrical and Information Engineering, Hunan University, Changsha, China, in 2017 and 2022, respectively.

Since October 2022, he has been a Research Fellow with Energy Research Institute, Nanyang Technological University, Singapore. His main research interests include the medium voltage dc system, dual active bridge converters, resonant converters, energy router, and the application of artificial intelligence in power electronics.

Dr. Xiao was the Session Chair for the 49th Annual Conference of the IEEE Industrial Electronics Society.

Fei Deng (Member, IEEE) received the B.E. and Ph.D. degrees in electrical engineering from Northwestern Polytechnical University, Xi'an, China, in 2015 and in 2021, respectively.

From 2018 to 2020, he was a Visiting Student with the University of Padova, Vicenza, Italy. Since 2022, he has been a Research Fellow with the Energy Research Institute, Nanyang Technological University, Singapore. His research interests include modeling, control, and analysis of power converters, and power management in microgrids.

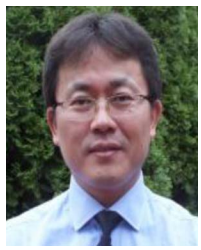

Caisheng Wang (Senior Member, IEEE) received the B.S. and M.S. degrees in electrical engineering from Chongqing University, Chongqing, China, in 1994 and 1997, respectively, and the Ph.D. degree in electrical engineering from Montana State University, Bozeman, MT, USA, in 2006.

From 1997 to 2002, he worked as an Electrical Engineer and then as a Vice Department Chair with Zhejiang Electric Power Test & Research Institute, Hangzhou, China. In 2006, he joined Wayne State University, where he is currently a Professor with the Department of Electrical and Computer Engineering. His current research interests include modeling and control of power systems and electric vehicles, power electronics, energy storage devices, distributed generation and microgrids, alternative/hybrid energy power generation systems, and fault diagnosis and on-line monitoring of electric apparatus.

Dr. Wang is an Associate Editor of IEEE ELECTRIFICATION MAGAZINE and was an Associate Editor of several other journals, including IEEE TRANSACTIONS ON SMART GRID.

Yi Tang (Senior Member, IEEE) received the B.Eng. degree in electrical engineering from Wuhan University, Wuhan, China, in 2007, and the M.Sc. and Ph.D. degrees in electrical engineering from the School of Electrical and Electronic Engineering, Nanyang Technological University, Singapore, in 2008 and 2011, respectively.

From 2011 to 2013, he was a Senior Application Engineer with Infineon Technologies Asia Pacific, Singapore. From 2013 to 2015, he was a Postdoctoral Research Fellow with Aalborg University, Aalborg, Denmark. Since March 2015, he has been with Nanyang Technological University, Singapore, where he is currently a tenured Associate Professor. His research interests include power electronics and its applications in smart grid and e-mobility systems.

Dr. Tang was the recipient of the Infineon Top Inventor Award in 2012, the Early Career Teaching Excellence Award in 2017, and four IEEE Prize Paper Awards. He serves as an Associate Editor for IEEE TRANSACTIONS ON POWER ELECTRONICS and the IEEE JOURNAL OF EMERGING AND SELECTED TOPICS IN POWER ELECTRONICS.